Spectroscopic and Kinetic Study of the Cl−S(CH$_3$)$_2$ Adduct

S. P. Urbanski[†,‡] and P. H. Wine*[,‡,§]

School of Earth and Atmospheric Sciences and School of Chemistry and Biochemistry, Georgia Institute of Technology, Atlanta, Georgia 30332

Received: July 29, 1999; In Final Form: October 18, 1999

Time-resolved ultraviolet−visible absorption spectroscopy has been coupled with 248 nm laser flash photolysis of Cl_2CO in the presence of DMS (CH_3SCH_3) (and in some cases O_2, NO, or NO_2) to generate the Cl−S(CH$_3$)$_2$ radical adduct in the gas phase and study the spectroscopy and kinetics of this species. The Cl−S(CH$_3$)$_2$ adduct was found to possess a strong, broad, unstructured absorption spectrum, extending from ca. 450 nm to below 280 nm with $\sigma_{max} = (3.48 \pm 1.04) \times 10^{-17}$ cm^2 molec^{-1} at $\lambda_{max} \approx 340$ nm. Reaction of the adduct with O_2 was not observed, and our data suggest that the rate coefficient for this reaction at 298 K is less than 4×10^{-18} cm^3 molec^{-1} s^{-1}. Rate coefficients for Cl−S(CH$_3$)$_2$ reactions with NO (k_{NO}) and NO_2 (k_{NO_2}) were measured at 155 Torr total pressure and room temperature, and were found to be $k_{NO} = (1.19 \pm 0.18) \times 10^{-11}$ cm^3 molec^{-1} s^{-1} and $k_{NO_2} = (2.70 \pm 0.41) \times 10^{-11}$ cm^3 molec^{-1} s^{-1}, where the uncertainties are estimates of accuracy at the 95% confidence level. The spectroscopic and kinetic data are used to evaluate the relative importance of possible atmospheric destruction mechanisms for Cl−S(CH$_3$)$_2$.

Introduction

Dimethyl sulfide (CH_3SCH_3, DMS) is produced by the biological activity of phytoplankton in the ocean, and its release from the oceans is the largest natural source of atmospheric sulfur on a global scale and the single largest source of atmospheric sulfur in the Southern Hemisphere.[1,2] In the remote marine boundary layer, where contributions from anthropogenic SO_2 are small, the gas-phase oxidation of DMS is the most important source of oxidized sulfur compounds such as SO_2, methanesulfonic acid (MSA), dimethyl sulfoxide (DMSO), dimethyl sulfone ($DMSO_2$), and H_2SO_4. It has been proposed that, through the production of sulfuric acid, the atmospheric oxidation of DMS may impact aerosol production and cloud formation processes, and hence the earth's radiation budget.[3] As a result of the potential role DMS may play in the global climate system, the oxidation mechanism of this compound has received considerable attention in recent years.

The primary oxidants in the marine boundary layer are hydroxyl radical and nitrate radical. Reaction with OH in the daytime and NO_3 at night are believed to be the most important processes initiating the oxidation of DMS in the atmosphere.[1] The importance of Cl atoms as an oxidant in the remote marine boundary layer is a subject of ongoing debate. A growing body of evidence suggests that reaction with Cl atoms may constitute a significant contribution to the oxidation of DMS in some atmospheric environments.

Many nonmethane hydrocarbons (NMHC) react much more rapidly with Cl atoms than with OH radicals,[4] and due to this significant difference in the reactivities of certain NMHC, measured temporal changes in the concentrations of NMHC may be used to infer the ambient concentrations of Cl atoms (see for example Jobson et al.[5]). Some field studies measuring NMHC have yielded evidence of Cl atom chemistry in the marine boundary layer.[5−7] Atmospheric field measurements employing mist chamber techniques, which indirectly measure Cl_2 and HOCl, have indicated Cl_2 and HOCl levels in the range of <26 to 254 pptv Cl in the coastal marine boundary layer.[8] Measurements of "total photolyzable chlorine" in the Arctic marine boundary layer around polar sunrise indicate mixing ratios ranging from <9 to 100 pptv (reported as Cl_2).[9] Most recently, molecular chlorine has been directly observed in coastal marine air. Employing a high-pressure chemical ionization mass spectrometry technique, Spicer et al.[10] directly measured Cl_2 levels ranging from <10 to 150 pptv. A modeling study conducted by Spicer et al.[10] found that, shortly after sunrise, the oxidation rate of DMS by Cl could, under favorable conditions, be an order of magnitude faster than rate of oxidation by OH.

While a limited number of field studies suggest that Cl atoms play an important local role in marine boundary layer chemistry, the importance of Cl chemistry on a global scale remains uncertain. Evidence does exist suggesting that, on a global scale, in the remote marine environment, the importance of Cl atoms as an oxidant is minimal. Two modeling studies conducted using real-time measurements of OH, DMS, and SO_2, and observed DMS and SO_2 diurnal trends, indicate that reaction with Cl constitutes less than 15% of DMS removal in the remote equatorial Pacific boundary layer.[12] A global 2-D tropospheric modeling study by Singh et al.[13] predicted atmospheric C_2Cl_4 concentration fields using OH chemistry alone, and by comparison with actual C_2Cl_4 observations, concluded that, on a global average, Cl atoms account for only a few percent of total DMS removal.

Because of the conflicting evidence regarding Cl atom chemistry, the importance of Cl in initiating DMS oxidation on a global scale remains speculative. A mechanism capable of efficiently generating photolytically active inorganic chlorine compounds in the remote marine environment has yet to be firmly established. The uptake of N_2O_5 gas by sea-salt aerosols is believed to generate gas-phase $ClNO_2$; however, a recent modeling study by Erickson et al.[11] suggests that global production of $ClNO_2$ by aerosol processes is of significance only in regions of the marine boundary layer impacted by

* To whom correspondence should be addressed.
† Present address: Department of Earth and Planetary Sciences, Harvard University, Cambridge, MA 02138.
‡ School of Earth and Atmospheric Sciences.
§ School of Chemistry and Biochemistry.

10.1021/jp992682m CCC: $18.00
Published on Web 11/18/1999

pollution (regions with sufficient nitrogen oxides). The aforementioned field studies (mist chamber measurements, the Arctic studies, and the recent direct measurement of molecular chlorine) all suggest that other aerosol processes which produce Cl_2, and possibly HOCl, are active, at least locally, in the marine boundary layer. Depending on the mechanisms responsible for generating the photolytically active inorganic chlorine observed in field studies, Cl atom chemistry could be more important than previously believed and may be of significance in initiating DMS oxidation on a global scale.

Reaction of Cl with DMS. The potential importance of Cl atoms in initiating the atmospheric oxidation of DMS has led to several laboratory and ab initio studies of the Cl + DMS reaction. The reaction of Cl with DMS proceeds via two distinct channels, a pressure-dependent adduct-forming channel and a pressure-independent channel.[14] The pressure dependence study of Stickel et al.[14] employed time-resolved resonance fluorescence detection of Cl atoms and determined that the Cl + DMS rate coefficient increases from a low-pressure limit value of ca. 1.8×10^{-10} cm^3 molec^{-1} s^{-1} to a value of $(3.3 \pm 0.5) \times 10^{-10}$ cm^3 molec^{-1} s^{-1} at 700 Torr of N_2; the rate coefficient for the pressure-dependent channel appears to approach its high-pressure limit between 150 and 700 Torr.[14] Two other rate coefficient measurements, obtained employing relative rate techniques, report values of $(3.61 \pm 0.21) \times 10^{-10}$ cm^3 molec^{-1} s^{-1} [15] and $(3.2 \pm 0.30) \times 10^{-10}$ cm^3 molec^{-1} s^{-1} [16] in 1 atm N_2 at room temperature. The study of Kinnison et al.[15] observed a small increase in the rate coefficient in the presence of O_2, with $k = (4.10 \pm 0.17) \times 10^{-10}$ cm^3 molec^{-1} s^{-1} in 1 atm synthetic air.

The study of Stickel et al. also employed time-resolved tunable diode laser absorption spectroscopic (TDLAS) detection of HCl and found that the yield of HCl increases with decreasing pressure, approaching unity as $P \rightarrow 0$. At 200 Torr, where the *P*-dependent channel appears to have leveled off, the HCl yield is ca. 50%.[14] The findings of Stickel et al.[14] are supported by the discharge-flow mass spectrometry study of Butkovskaya and LeBras,[17] which observed HCl + CH_3SCH_2 as the only reaction channel in 1 Torr of He. Possible channels for the Cl + DMS reaction include:

$$\mathrm{Cl} + \mathrm{CH_3SCH_3} \rightarrow \mathrm{HCl} + \mathrm{CH_3SCH_2} \quad (1a)$$

$$\mathrm{Cl} + \mathrm{CH_3SCH_3} \rightarrow [\mathrm{Cl{-}S(CH_3)_2}]^* \quad (1b)$$

$$[\mathrm{Cl{-}S(CH_3)_2}]^* + \mathrm{M} \rightarrow \mathrm{CH_3SCl} + \mathrm{CH_3} + \mathrm{M} \quad (1c)$$

$$[\mathrm{Cl{-}S(CH_3)_2}]^* + \mathrm{M} \rightarrow \mathrm{CH_3Cl} + \mathrm{CH_3S} + \mathrm{M} \quad (1d)$$

Zhao et al.[18] employed TDLAS detection of CH_3 to place an upper limit of 2% on the yield of methyl (1b). A CH_3Cl yield of $(1.34 \pm 0.07) \times 10^{-3}$ was reported by Langer et al.[19] The investigation of Stickel et al. demonstrated that the stabilized adduct (1d) does not dissociate to Cl or HCl on the millisecond time scale (the time scale of their experiments). The experiments of Langer et al.[19] were conducted in 1 atm air and show that adduct decomposition to CH_3Cl and CH_3S is unimportant under atmospheric conditions. Thus, despite several laboratory studies, the atmospheric disposition of half the Cl + DMS reaction, i.e., the fate of the Cl−S(CH$_3$)$_2$ adduct, remains highly uncertain. The goal of the current study is to further our understanding of the atmospheric fate of the Cl−S(CH$_3$)$_2$ adduct.

While the Cl−S(CH$_3$)$_2$ adduct has not been directly observed in any previously published laboratory studies, ab initio investigations support its existence. Theoretical studies suggest that the Cl−S(CH$_3$)$_2$ adduct is formed via a two-center−three-electron bond, with the spin density higher on the Cl atom than on the S atom, and predict that the adduct is stable with respect to reactants by 52−90 kJ mol^{-1}.[20−23] The reaction of Br with DMS forms a weakly bound adduct with a lifetime toward unimolecular decomposition of 2.5 ms (263 K) to 100 μs (310 K) at 50 Torr total pressure.[24] The Br−S(CH$_3$)$_2$ adduct has been directly observed in the laboratory by ultraviolet−visible (UV−vis) absorption spectroscopy and is reported to possess a strong, broad, unstructured absorption spectrum with a maximum around 365 nm.[24,25] By using time-resolved resonance fluorescence detection of bromine atoms, Wine et al.[24] observed the kinetics of the approach to equilibrium as a function of temperature and determined a Br−S bond strength of 59 ± 8 kJ mol^{-1} for the Br−S(CH$_3$)$_2$ adduct.

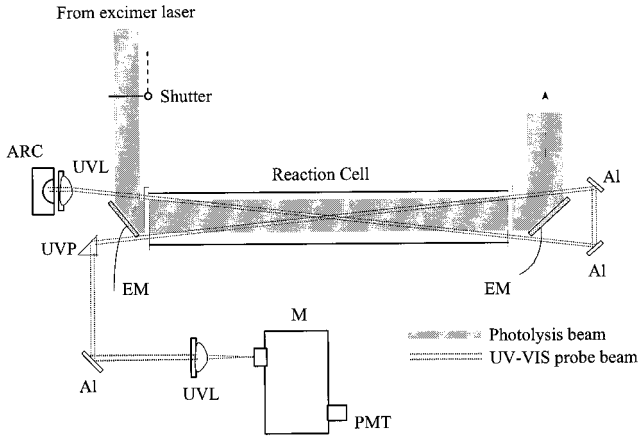

Figure 1. Laser flash photolysis/UV−vis absorption spectroscopy apparatus: ARC = HgXe arc lamp; UVL = UV grade fused silica lens; EM = excimer laser mirror; Al = UV enhanced aluminum mirror; UVP = UV grade fused silica prism; M = monochromator; PMT = photomultiplier tube.

We have employed laser flash photolytic (LFP) generation of Cl in the presence of DMS to investigate the spectroscopy and kinetics of the Cl−S(CH$_3$)$_2$ adduct. The Cl−S(CH$_3$)$_2$ adduct has been positively identified and its UV−vis absorption spectrum has been measured. To determine the atmospheric fate the adduct, time-resolved UV−vis absorption spectroscopy has been utilized to explore adduct reactivity toward O_2, NO, and NO_2. Additionally, the UV−vis absorption spectrum of the adduct has been used to calculate its atmospheric lifetime with respect to photolysis.

Experimental Technique

The laser flash photolysis (LFP)/UV−vis absorption spectroscopy apparatus used in the spectroscopic and kinetic studies of the Cl−S(CH$_3$)$_2$ adduct is depicted in Figure 1. The major elements are an excimer photolysis laser, a high-pressure HgXe arc lamp, a monochromator and photomultiplier tube (PMT), a Pyrex reaction cell (100 cm long, 40 mm i.d.), and numerous optical components used to manipulate and align the excimer laser photolysis beam and the UV−vis probe beam. As depicted in Figure 1, the UV−vis probe beam was passed through the reaction cell twice. Because the mirrors used to direct the photolysis beam through the reaction cell were inefficient transmitters of UV light, it was necessary to direct the UV−vis probe beam through the reaction cell at an angle relative to the horizontal axes of the collinearly aligned photolysis beam and reaction cell (see Figure 1).

A Lambda Physik Compex 102 KrF excimer laser served as the photolysis laser and delivered a typical fluence of 25−35

mJ cm^{-2} pulse^{-1} in the center of the reaction cell at a wavelength of 248 nm with a pulse duration of ca. 20 ns. The photolysis beam covered an area of 3.5 cm × 1.5 cm in the center of the reaction cell where variations of the cross-sectional spatial intensity in the photolysis beam were measured to be less than 20%. The internal energy meter of the excimer laser was used to continuously monitor the photolysis laser energy. The photolysis energy in the center of the reaction cell was determined from an absolute calibration of the internal energy meter using a Scientech disk calorimeter (model 214). Variations in the shot to shot laser pulse energy were typically less than 2%.

The UV−vis light source was a high-pressure 200 W HgXe arc lamp. Time-resolved monitoring of the probe beam intensity was achieved using a 0.22 m grating monochromator and PMT. The monochromator entrance and exit slits were set at 1000 μm, providing a resolution of 3.7 nm (fwhm). The monochromator wavelength setting was calibrated using a Hg pen ray lamp, placed in the position of the HgXe arc lamp. The Hg atomic lines at 253.65 and 404.65 nm were used to calibrate the monochromator wavelength dial and measure the monochromator resolution. The monochromator resolution was independent of wavelength. The time-dependent current output by the PMT was routed through a fixed resistor, and the resulting dc voltage was passed through an amplifier (Data Precision model D1000) prior to digitization, averaging, and storage accomplished with an 8 bit digital signal averager. Depending on the required time resolution, the RC time constant of the circuit (PMT/coaxial cable/resistor) was varied from 1 to 10 μs by changing the resistor.

As discussed above, the optical properties of the mirrors used to direct the photolysis beam through the reaction cell necessitated an orientation of the UV−vis probe beam that was skewed relative to the photolysis beam axis. As a result, the UV−vis probe beam was overlapped by the photolysis beam for only part of its passage through the reaction cell (see Figure 1). It was thus necessary to empirically determine the effective UV−vis probe path length, i.e., the distance over which the probe beam passed through the volume of the reaction cell exposed to the photolysis beam. Measurement of the UV−vis probe beam effective path length, l_{eff}, was achieved by photolyzing Cl_2CO in the presence of CH_4 and O_2:[4]

$$Cl_2CO + h\nu \rightarrow Cl + Cl + CO \quad (2)$$

$$Cl + CH_4 \rightarrow CH_3 + HCl \quad (3)$$

$$CH_3 + O_2 + M \rightarrow CH_3OO + M \quad (4)$$

The CH_3OO radicals were monitored at 265 nm. The initial Cl atom concentration, and hence the peak CH_3OO concentration, was varied by varying the Cl_2CO concentration and the excimer laser fluence. Plots of the peak CH_3OO absorbance versus initial Cl concentration were linear, and the slope, obtained from a linear least-squares fit to data, yielded the effective path length, l_{eff} = slope/σ, where σ is the CH_3OO absorption cross section at 265 nm ($\sigma = 2.48 \times 10^{-18}$ cm^2 molec^{-1}).[26] Effective path length measurements were conducted using ca. 45 Torr of CH_4, 20 Torr of O_2, a total pressure of 90 Torr, and initial Cl concentrations of $1-8 \times 10^{13}$ molec cm^{-3}. At the highest initial Cl atom concentrations, it was necessary to make a small correction for the reaction of Cl with CH_3OO; this correction never exceeded 10%.

The Cl−S(CH$_3$)$_2$ adduct was generated by photolyzing Cl_2CO in the presence of DMS in N_2 and/or O_2 buffer gas. Absorption cross sections for Cl_2CO and DMS at 248 nm are, in units of 10^{-20} cm^2, 8.93[18] and 1.28,[27] respectively; hence, for a typical photolysis fluence of 30 mJ cm^{-2} pulse^{-1}, ∼0.3% of Cl_2CO and ∼0.05% of DMS in the laser path are photolyzed. All experiments were conducted under "slow flow" conditions; that is, the linear flow rate of the reaction mixture through the reaction cell was sufficient to completely replenish the entire volume of the reaction cell between photolysis laser pulses. The concentrations of both DMS and Cl_2CO were measured in situ by UV photometry and by mass flow measurements. The in situ photometry measurements were conducted using a Zn pen ray lamp, 214 nm interference band-pass filter, and a side-on PMT. The cross sections used to convert 213.9 nm absorbances to concentrations were $\sigma_{DMS} = 1.70 \times 10^{-18}$ cm^2 molec^{-1} [27] and $\sigma_{Cl_2CO} = 1.26 \times 10^{-19}$ cm^2 molec^{-1}.[4] In the kinetics experiments, the concentrations of NO and NO_2 were determined from mass flow measurements. A certified NO/N_2 mixture (1.87% NO) was used to supply NO. Nitrogen dioxide was transferred into a 12 L Pyrex bulb and diluted with O_2 (1.27% NO_2 in O_2). The NO_2 mole fraction of the NO_2/O_2 mixture was measured using UV photometry.

The pure gases used in this study were obtained from Air Products Specialty Gases (O_2, N_2), Matheson Gas Products (Cl_2CO, NO_2), and Spectra Gases (CH_4) and had the following stated minimum purities: N_2, 99.999%; O_2, 99.994%; Cl_2CO, 99.0%; NO_2, 99.5%; CH_4, 99.995%. The NO was supplied by Matheson Gas Products as an analyzed mixture, 1.87% NO in N_2. The N_2, O_2, NO_2, NO/N_2 were used as supplied. The Cl_2CO was degassed at 77 K prior to use. The dimethyl sulfide was acquired from Aldrich Chemical Corp. and had a stated minimum purity of 99.0%. The dimethyl sulfide was transferred under N_2 into vials fitted with high-vacuum stopcocks and degassed repeatedly at 77 K before use.

Results

Adduct Spectroscopy. When Cl_2CO was photolyzed in the presence of DMS, absorption of the UV−vis probe beam was observed throughout the 270 to 450 nm spectral region. Absorption of the UV−vis probe beam was observed only when both DMS and Cl_2CO were present. The observed absorbance (Abs) decayed rapidly with time according to second-order kinetics, i.e., plots of (Abs)$^{-1}$ versus time were linear. The peak absorbance for each experiment, Abs_0, was determined by plotting (Abs)$^{-1}$ versus time and extrapolating (Abs)$^{-1}$ back to $t = 0$ using a linear least-squares fit to the absorbance data.

Adduct Identification. The study of Stickel et al.[14] demonstrated that the yield of the adduct channel increases with pressure (the observed HCl yield decreased from ca. 85% at 5 Torr of N_2 to slightly over 50% between 100 and 200 Torr of N_2). Thus, the UV−vis absorption observed following the photolysis of Cl_2CO/DMS mixtures, if attributable to the Cl−S(CH$_3$)$_2$ adduct, should vary with pressure accordingly. The product of the H− abstraction channel, CH_3SCH_2, also absorbs the UV−vis probe radiation; the absorption spectra of CH_3SCH_2 and CH_3SCH_2OO have been reported by Wallington et al.[28] By varying the total pressure and detection wavelength, it was possible to identify absorption attributable to Cl−S(CH$_3$)$_2$. For example, at 2.7 Torr, significant absorption was observed at 360 nm, where CH_3SCH_2 absorption is negligible. Increasing the pressure, and thus the adduct yield, resulted in a dramatic increase in absorption at 360 nm. The ratio of the "effective cross section", σ_{eff}, ($\sigma_{eff} = Abs_0/l_{eff}$ [Cl]$_0$) at 360 nm measured at high and low pressure, σ_{eff}(2.7 Torr)/σ_{eff}(155 Torr) ≈ 0.25, is in good agreement with the adduct yield ratio calculated using

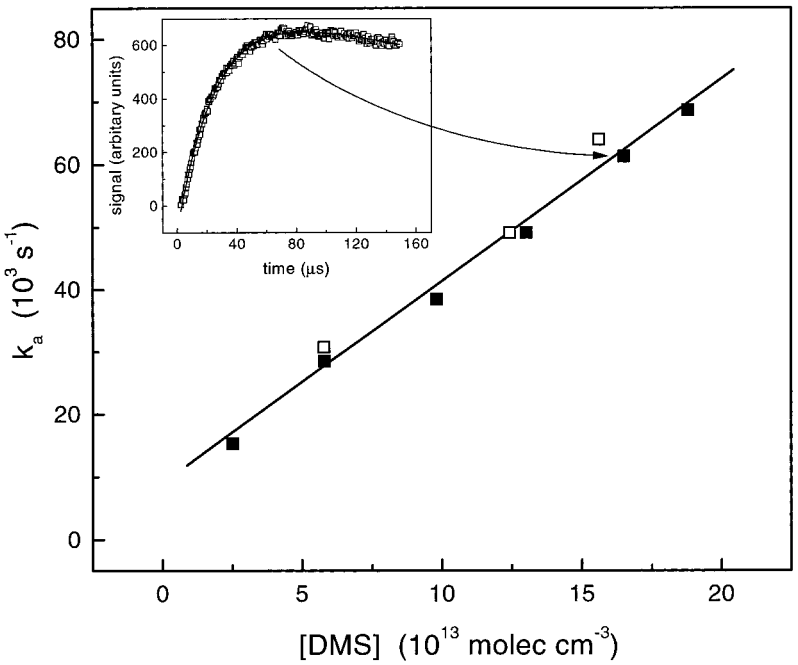

Figure 2. Pseudo-first-order adduct appearance rate (k_a) versus [DMS] for the Cl + DMS reaction at $P = 155$ Torr and $T = 294$ K in (■) O_2 buffer gas and (open square: □) N_2 buffer gas. Line is the linear least-squares fit to the data. Best-fit slope is $(3.2 \pm 0.3) \times 10^{-10}$ cm^3 $molec^{-1}$ s^{-1} (uncertainty 2σ, precision only). Inset: typical $Cl-S(CH_3)_2$ appearance temporal profile. Solid line is a double-exponential fit to the data (see text). Reagent concentrations are (in units of 10^{13} molec cm^{-3}) [DMS] = 165, [Cl_2CO] = 290, and $[Cl]_0 = 1.9$; $P = 155$ Torr (O_2 buffer gas) and $T = 294$ K.

the HCl yields reported by Stickel et al., $\Phi(5\text{ Torr})/\Phi(150\text{ Torr}) \approx 0.27$. The observed variation of σ_{eff} with pressure is consistent with absorption by the product of the Cl + DMS adduct-forming channel, $Cl-S(CH_3)_2$.

Further evidence verifying the identity of the absorbing species was obtained by measuring its appearance rate. By utilizing sufficiently low DMS concentrations, the appearance rate of the absorbing species was reduced to less than 80 000 s^{-1}, and absorption temporal profiles were recorded and analyzed using a nonlinear least-squares fit to the sum of an exponential rise and an exponential decay (see Figure 2). In this set of experiments, $Cl-S(CH_3)_2$ disappearance resulted primarily from adduct−radical reactions and was not strictly a first-order loss process. The variable for the first-order $Cl-S(CH_3)_2$ disappearance, k_d, is thus a parametrized $Cl-S(CH_3)_2$ disappearance rate coefficient rather than the sum of actual loss processes which are quantitatively attributable to specific first-order reactions. Because the $Cl-S(CH_3)_2$ loss rates are slow compared to the rapid rate of $Cl-S(CH_3)_2$ appearance, the parametrization of the $Cl-S(CH_3)_2$ disappearance as a first-order process does not seriously impact the reliability of the analysis. As may be seen from the inset in Figure 2, the fits were of excellent quality. Pseudo-first-order appearance rates (k_a) were measured at 365 nm, in O_2 and N_2 buffer gases. Plots of k_a vs DMS concentration were linear over the range of DMS concentrations employed (see Figure 2). The linearity of the k_a vs DMS concentration plot up to the fastest appearance rate measured (ca. 70 000 s^{-1}) demonstrates that the rate-limiting step in production of the absorbing species was the Cl + DMS reaction under the conditions investigated. The slope of the k_a vs DMS concentration plot (see Figure 2) yields the second-order rate coefficient $k_1 = (3.2 \pm 0.3) \times 10^{-10}$ cm^3 $molecule^{-1}$ s^{-1} at 298 K and 155 Torr total pressure, where the uncertainty is 2σ and represents precision only. The value measured here for k_1 at 155 Torr is in good agreement with those reported in the literature[14−16] (see above), indicating that the species being observed is indeed the $Cl-S(CH_3)_2$ adduct formed from the reaction of Cl with DMS.

Adduct Absorption Spectrum. The absorption spectrum of the $Cl-S(CH_3)_2$ adduct was measured at 155 Torr total pressure (mostly O_2 buffer). A total pressure of 155 Torr was chosen to maximize the adduct yield and was based on the study of Stickel et al.[14] which indicates that the adduct yield levels off between 100 and 200 Torr. Because the product of the H-abstraction channel, CH_3SCH_2, absorbs light in the 260 to 350 nm region, the experiments were conducted using ca. 130 Torr of O_2 which converted CH_3SCH_2 into CH_3SCH_2OO in <0.5 μs.[28,29] The CH_3SCH_2OO absorption spectrum peaks at 240 nm, and the CH_3SCH_2OO absorption cross section is negligible at wavelengths longer than 280 nm.[28] Thus, the conversion of CH_3SCH_2 into CH_3SCH_2OO largely eliminated spectral interferences accompanying the adduct production chemistry.

An additional minor complication to the adduct spectrum measurements was the formation of a long-lived (i.e., persistent at 40+ ms) product(s) which absorbed the probe beam at wavelengths below ca. 320 nm. This absorption was observed in both N_2 and O_2 buffer gases and the absorbance increased with pressure, suggesting that the product(s) was produced in a reaction involving $Cl-S(CH_3)_2$. The residual absorbance increased with decreasing wavelength down to the lowest wavelength monitored (265 nm). The ratio of the residual absorbance to the adduct absorbance increased from ca. 0.02 at 315 nm to ca. 1.4 at 280 nm. This long-lived absorption and the potential source(s) are discussed below. The absorption temporal profiles were corrected for the presence of the long-lived absorbing product(s) by subtracting the observed long time absorption, i.e., the post flash baseline, from the entire post flash absorption profile.

Adduct absorption cross section measurements were carried out at 155 Torr total pressure (130 Torr of O_2) and room temperature with typical reagent concentrations of (in units of 10^{13} molec cm^{-3}) [DMS] = 100−150, [Cl_2CO] = 400−700,

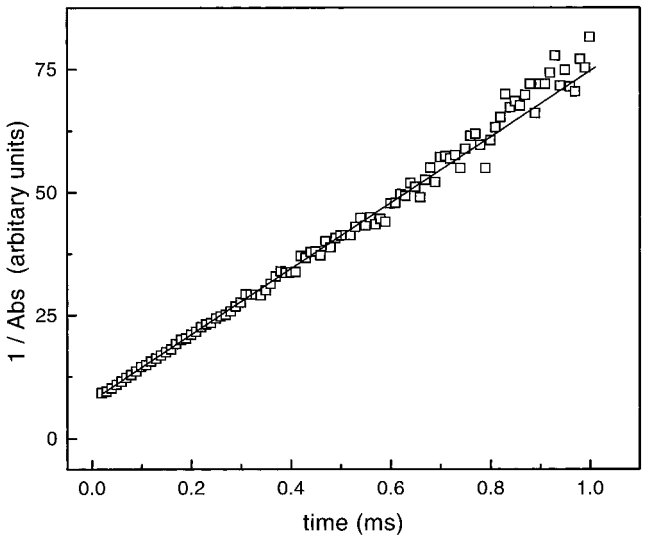

Figure 3. Cl−S(CH$_3$)$_2$ absorbance temporal profile plotted as 1/absorbance (1/Abs) versus time. Data acquired via 248 nm laser flash photolysis of DMS/Cl$_2$CO/N$_2$/O$_2$ gas mixture. Total pressure = 159 Torr and T = 296 K. Line is a linear least-squares fit to the data. Concentrations are (in units of 10^{13} molec cm^{-3}) [DMS] = 137, [Cl$_2$CO] = 1020, and [Cl]$_0$ = 5.8. Best-fit intercept is Abs$_0$ = 0.130 ± 0.0055 (uncertainty is 2σ, precision only).

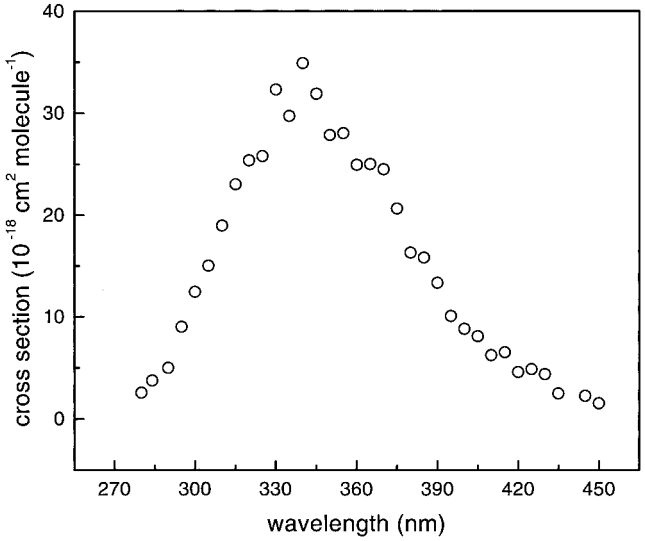

Figure 4. UV−vis absorption spectrum of the Cl−S(CH$_3$)$_2$ adduct.

and [Cl]$_0$ = 3−5. Each cross section measurement involved averaging 50−125 photolysis laser pulses. To verify reproducibility, multiple cross section measurements were taken at several wavelengths on separate days. The adduct cross section for each measurement was determined from the data using

$$\sigma_\lambda = \frac{\mathrm{Abs}_0}{l_{\mathrm{eff}}\Phi_{\mathrm{adduct}}[\mathrm{Cl}]_0} \qquad \text{(I)}$$

where Abs$_0$, l_{eff}, and [Cl]$_0$ are as defined previously and Φ_{adduct} (=0.45) is the adduct yield from the Cl + DMS reaction.[14] Data from a typical cross section measurement are shown in Figure 3. The entire adduct spectrum measured in this study is given in Figure 4 and Table 1. At wavelengths where multiple cross section measurements were taken, the mean of the measurements was used.

The Cl−S(CH$_3$)$_2$ absorption spectrum was also measured in 155 Torr of N$_2$. The absorption measurements obtained in N$_2$ buffer had to be corrected for CH$_3$SCH$_2$ absorption using the CH$_3$SCH$_2$ cross section data reported by Wallington et al.[28] and were thus less precise than those obtained in O$_2$ buffer gas. The absorption cross sections measured in N$_2$ agreed with those measured in O$_2$, within the combined uncertainties of the individual measurements. The agreement between the absorption spectra measured in N$_2$ buffer gas and O$_2$ buffer gas lends further support to our conclusion that the species observed in this study is in fact the Cl−S(CH$_3$)$_2$ adduct.

Additional measurements of the Cl−S(CH$_3$)$_2$ absorption cross section were made at 340 and 365 nm. These wavelengths were chosen because 340 nm is approximately the peak of the observed absorption spectrum and 365 nm was the wavelength chosen to monitor the adduct for kinetics studies. A monitoring wavelength of 365 nm was chosen for the kinetics experiments in order to avoid spectral interferences from the unidentified long-lived species and CH$_3$SCH$_2$, and because the combination of adduct absorption cross section and probe beam intensity (which was greatest at ca. 365 nm) gave the best signal-to-noise ratio. The additional cross section measurements were also made at 155 Torr total pressure (130 Torr of O$_2$) and room temperature. Consideration of uncertainties in the adduct yield, the effective path length, the excimer laser internal power meter calibration, the measured [Cl$_2$CO], the Cl$_2$CO absorption cross section at 248 nm, and Abs$_0$, the parameters which must be known to obtain the adduct cross section, leads to an estimate of ±30% for the accuracy of the measured cross sections at 340 and 365 nm (95% confidence level). The absorption cross section at each wavelength and the associated uncertainties are

$$\sigma_{340} = (3.48 \pm 1.04) \times 10^{-17}\ \mathrm{cm}^2\ \mathrm{molec}^{-1}$$

and

$$\sigma_{365} = (2.50 \pm 0.75) \times 10^{-17}\ \mathrm{cm}^2\ \mathrm{molec}^{-1}$$

Adduct Kinetics. In the marine boundary layer, reaction with O$_2$, NO, NO$_2$, and O$_3$, as well as unimolecular decomposition and photolysis, may all contribute to Cl−S(CH$_3$)$_2$ removal. The kinetics of the Cl−S(CH$_3$)$_2$ adduct reactivity toward O$_2$, NO, and NO$_2$ have been investigated in an attempt to determine the fate of the adduct under atmospheric conditions. In the atmosphere, O$_2$ is the most abundant reactive species and is the most likely candidate for reactive adduct removal. The initial investigation of Cl−S(CH$_3$)$_2$ spectroscopy revealed that, in the presence of 130 Torr of O$_2$, observed adduct decay temporal profiles were nonexponential and obeyed second-order kinetics. This observation indicates that reaction with O$_2$ was not the dominant removal process for the adduct, but rather that adduct loss was dominated by adduct−radical chemistry. To better assess the role of side reactions in the adduct kinetic studies, an attempt to understand the adduct self-reaction and adduct cross reactions with CH$_3$SCH$_2$ and CH$_3$SCH$_2$OO was also pursued.

As mentioned above, when Cl$_2$CO was photolyzed in the presence of DMS, the second-order decay of the adduct was followed by formation of a long-lived (i.e., persistent at 40+ ms) species which absorbed light at wavelengths below ca. 320 nm. This residual absorption was observed in both N$_2$ buffer gas and O$_2$ buffer gas. The wavelength dependencies and magnitudes of the residual absorbances in O$_2$ buffer gas and N$_2$ buffer gas were similar, strongly suggesting that the absorption observed in both buffer gases resulted from the same species. The long-lived absorption increased with pressure indicating that the concentration of the absorbing species

TABLE 1: Cl−S(CH$_3$)$_2$ Adduct Absorption Spectrum

wavelength (nm)	cross section (10^{-18} cm^2 molec^{-1})	wavelength (nm)	cross section (10^{-18} cm^2 molec^{-1})	wavelength (nm)	cross section (10^{-18} cm^2 molec^{-1})
280	2.54	340	34.8	400	8.80
284	3.72	345	31.9	405	8.07
290	4.96	350	27.8	410	6.21
295	8.98	355	28.0	415	6.48
300	12.4	360	24.9	420	4.57
305	15.0	365	25.0	425	4.84
310	18.9	370	24.4	430	4.34
315	23.0	375	20.6	435	2.48
320	25.3	280	16.3	445	2.23
325	25.8	385	15.8	450	1.52
330	32.3	390	13.3		
335	29.7	395	10.0		

TABLE 2: Chemical Mechanism Employed for Analysis of Adduct Decay Temporal Profiles (See Text)

reaction	reaction	rate coefficient (cm^3 molec^{-1} s^{-1})	notes
1a	Cl + DMS → HCl + CH_3SCH_2	1.8×10^{-10}	*a*
1d	Cl + DMS + M → Cl-S(CH$_3$)$_2$ + M	1.3×10^{-10}	*a*,*b*
		0.4×10^{-10}	*a*,*b*
3	$CH_3SCH_2 + O_2 + M \rightarrow CH_3SCH_2OO + M$	1.0×10^{-12}	*c*
9	$CH_3SCH_2 + CH_3SCH_2 \rightarrow$ products	3.0×10^{-11}	*c*
11	$CH_3SCH_2OO + CH_3SCH_2OO \rightarrow 2\ CH_3S + O_2$	1.0×10^{-11}	*c*,*d*
7	Cl-S(CH$_3$)$_2$ + Cl-S(CH$_3$)$_2$ → products	k_7	*e*
8	Cl-S(CH$_3$)$_2$ + CH_3SCH_2 → products	k_8	*e*
10	Cl-S(CH$_3$)$_2$ + CH_3SCH_2OO → products	k_{10}	*e*

[a] Reference 14. [b] $k_{1b} = 1.3 \times 10^{-10}$ at high pressure (155 Torr) and 0.4×10^{-10} at low pressure (10 Torr). [c] Reference 28. [d] Reference 32. [e] Rate coefficients unknown (see text).

increased with increasing adduct concentration and was, therefore, a result of reactions involving the adduct.

Generation of the same product in O_2 buffer gas and N_2 buffer gas would require that the species either result from the adduct self-reaction or that the adduct reactions with CH_3SCH_2 and CH_3SCH_2OO produce a common product. Reaction pathways of potential importance in the Cl + DMS + N_2 (O_2) system are listed in Table 2. While the most likely products of reaction 7 would appear to be Cl_2 + DMS + DMS, Cl_2 does not absorb strongly in the region where the long-lived absorption was observed; hence, the adduct self-reaction must generate different products if it is responsible for the observed long-lived species.

The observed residual absorption could also result from reactions 8 and 10, if these reactions generate the same product. Likely products of reaction 8 are CH_3SCH_2Cl and DMS. The species chloromethyl methyl sulfide (CH_3SCH_2Cl) could conceivably also be produced via reaction 10,

$$Cl{-}S(CH_3)_2 + CH_3SCH_2OO \rightarrow CH_3SCH_2Cl + DMS + O_2 \quad (10a)$$

The literature is practically void of information regarding CH_3SCH_2Cl. An attempt was made to measure the gas-phase UV−vis absorption spectrum of CH_3SCH_2Cl (a liquid at room temperature, light-yellow in color); unfortunately the peculiar gas-phase behavior of this substance made it extremely difficult to handle, and our attempt to measure its UV−vis absorption spectrum was unsuccessful.

An analysis of the Cl + DMS + N_2 (O_2) system was conducted in an effort to estimate the values of k_7 and k_{10}. Decay curves of the adduct in N_2 buffer gas and O_2 buffer gas, at high pressure (155−180 Torr), were analyzed using the FACSIMILE program, a combination numerical integration and nonlinear least-squares fit routine[30] and the chemical mechanism listed in Table 2. The FACSIMILE routine, using the observed temporal profile of the absolute adduct concentration (determined from absorbance temporal profiles at 365 nm) and a rate coefficient of fixed value for reaction 9 or 11 (depending on whether O_2 was present), fit the observed data by varying the rate coefficients of the adduct self-reaction, k_7, and the adduct cross reaction, k_X ($k_X = k_8$ in N_2 buffer gas; $k_X = k_{10}$ in O_2 buffer gas). The analysis indicated that, in the presence of O_2, the adduct decay was consistent with adduct removal being dominated by self-reaction. The analysis suggests that the value of the adduct self-reaction rate coefficient is $k_7 \approx (1-2) \times 10^{-10}$ cm^3 molec^{-1} s^{-1} and that the adduct cross reaction with CH_3SCH_2OO is significantly slower with $k_7/k_{10} > 5$.

Adduct Decay in O_2. The spectroscopy studies of the Cl−S(CH$_3$)$_2$ adduct revealed that in 130 Torr of O_2 the adduct decay was not exponential, but rather second order, indicating that if the adduct is reactive toward O_2, the reaction 13 is very slow compared the adduct self-reaction and reaction 10.

$$Cl{-}S(CH_3)_2 + O_2 \rightarrow \text{products} \quad (13)$$

In an attempt to minimize the importance of adduct−radical reactions, experiments conducted to assess the reactivity of the adduct toward O_2 were carried out with very low radical concentrations ($[Cl]_0 = 3-4 \times 10^{12}$ molec cm^{-3} and peak adduct concentration $< 2 \times 10^{12}$ molec cm^{-3}).

Figure 5 shows plots of ln[adduct] versus time for data obtained at 360 Torr total pressure at two different O_2 partial pressures (11 and 339 Torr). Both plots in Figure 5 exhibit poor linearity, indicating adduct removal is not controlled by a purely pseudo-first-order process. A linear least-squares analysis of the last ca. 3.5 ms of the two data plots in Figure 5 gave pseudo-first-order adduct loss rates (k_d) of 162 ± 24 s^{-1} (11 Torr of O_2) and 208 ± 30 s^{-1} (339 Torr of O_2), where the uncertainties are 2σ and represent precision only. The value of k_d obtained from the data in the presence of 339 Torr of O_2 indicates that if the adduct loss resulted exclusively due to reaction with O_2, then the adduct + O_2 rate coefficient is ca. 2×10^{-17} cm^3 molec^{-1} s^{-1}. However, the similar adduct loss rate observed in the presence of only 11 Torr of O_2, and the poor linearity of the ln[adduct] versus time plots, demonstrates that adduct removal does not result exclusively from reaction with O_2 for

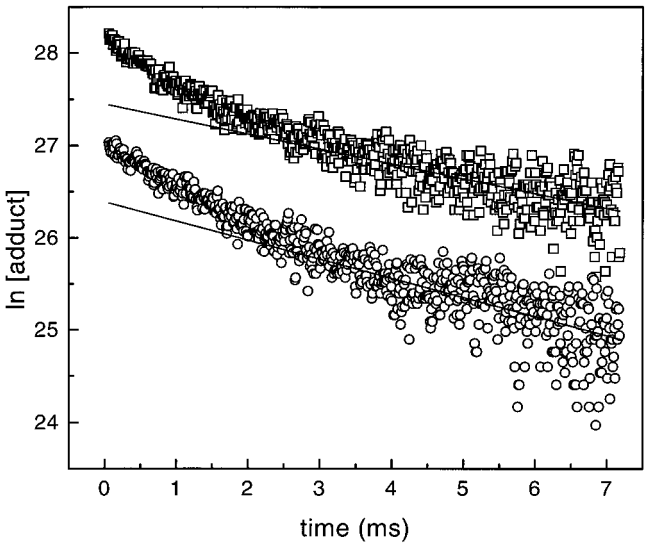

Figure 5. Cl−S(CH$_3$)$_2$ temporal profiles observed at low Cl−S(CH$_3$)$_2$ concentrations in the presence of very different concentrations of O_2. Data acquired via 248 nm laser flash photolysis of DMS/Cl_2CO/N_2/O_2 gas mixtures. Total pressure = 360 Torr and T = 296 K. Lines are linear least-squares fits to the later portion of the data (3.5 to 6.75 ms). Reagent concentrations are (in units of 10^{13} molec cm^{-3}) (○) [DMS] = 104, [Cl_2CO] = 105, [Cl]$_0$ = 0.36, [O_2] = 28000 and (□) [DMS] = 125, [Cl_2CO] = 113, [Cl]$_0$ = 0.39, [O_2] = 1 100 000. Best-fit slopes are (○) 162 ± 24 s^{-1} and (□) 208 ± 30 s^{-1} (uncertainty is 2σ, precision only). The data obtained with low [O_2] (○), has been off set by 1 unit for clarity of depiction.

the radical levels employed in these experiments. The fact that increasing the concentration of O_2 by 328 Torr resulted in only a 46 ± 40 s^{-1} increase in k_d suggests $k_{13} < 4 \times 10^{-18}$ cm^3 molec^{-1} s^{-1}. Additionally, part of the difference in k_d is likely a consequence of the slightly higher initial radical concentration (higher by ca. 8%) used in the 339 Torr of O_2 experiment. While the data establish that $k_{13} < 4.0 \times 10^{-18}$ cm^3 molec^{-1} s^{-1}, the actual rate coefficient for reaction 13 could be significantly less than the upper limit defined by the data.

Cl−S(CH$_3$)$_2$ + NO Reaction. The adduct reaction with NO was studied under pseudo-first-order conditions, i.e., with [adduct]$_0$ ≪ [NO]. The experiments were conducted at room temperature and 155 Torr of N_2. The NO was taken directly from a high-pressure storage cylinder containing an analyzed NO/N_2 mixture and the NO concentration was determined via mass flow measurements. The reagent concentrations (in units of molec cm^{-3}) used in these experiments were varied as follows: [Cl]$_0$ = (6−25) × 10^{12}; [DMS] = (10−16) × 10^{14}; [NO] = (2−40) × 10^{14}. A few experiments were carried out in 50 Torr of N_2 to discern any pressure dependence in the reaction.

In the presence of NO, the adduct temporal profiles obeyed simple first-order-kinetics, i.e., plots of ln(signal) versus time were linear (see inset Figure 6). The pseudo-first-order adduct decay rate (k_d) for each experiment was determined using a linear least-squares analysis of the ln(signal) versus time plot. The second-order rate coefficient for reaction 14 was evaluated from the slope of a plot of k_d versus NO concentration (see Figure 6).

$$\text{Cl}-\text{S(CH}_3\text{)}_2 + \text{NO} \rightarrow \text{products} \qquad (14)$$

The exponential adduct temporal profiles, the linear dependence of k_d on NO concentration, the approximately zero intercept of the k_d versus [NO] plot (1270 ± 2130 s^{-1}; uncertainty 2σ, precision only), and the invariance of k_d with respect to variations in the initial Cl concentration, excimer laser fluence, and pressure, demonstrates that bimolecular reaction with NO was the only important removal process for the adduct under the conditions of the experiments. The slope of the k_d versus [NO] plot (see Figure 6) defines the second-order rate coefficient $k_{14} = (1.19 \pm 0.09) \times 10^{-11}$ cm^3 molec^{-1} s^{-1} at 297 K, where the uncertainty is 2σ and represents precision only. On the basis of consideration of possible systematic errors (primarily in the determination of [NO]), we estimate that the absolute accuracy of the measured rate coefficient is ±15% at the 95% confidence level.

Cl−S(CH$_3$)$_2$ + NO$_2$ Reaction. The adduct reaction with NO_2 was also studied under pseudo-first-order conditions ([adduct]$_0$ ≪ [NO_2]). The experiments were conducted at room temperature and 155 Torr total pressure (mostly O_2). The NO_2 was taken from a 12 L Pyrex storage bulb containing an NO_2/O_2 mixture. The NO_2 concentration was determined via mass flow measurements. The mole fraction of NO_2 in the NO_2/O_2 mixture (1.27%) was determined using UV photometry. The reagent concentrations (in units of molec cm^{-3}) used in these experiments were varied as follows: [Cl]$_0$ = (10−14) × 10^{12}; [DMS] = (10−15) × 10^{14}; [NO_2] = (3−14) × 10^{14}.

In the presence of NO_2, the adduct temporal profiles obeyed simple first-order-kinetics, i.e., plots of ln(signal) versus time were linear (see inset Figure 7). The pseudo-first-order adduct decay rate (k_d) for each experiment was determined using a linear least-squares analysis of the ln(signal) versus time plot. The second-order rate coefficient for reaction 15 was evaluated from

$$\text{Cl}-\text{S(CH}_3\text{)}_2 + \text{NO}_2 \rightarrow \text{products} \qquad (15)$$

the slope of the k_d versus NO_2 concentration plot (see Figure 7). The exponential adduct temporal profiles, the linear dependence of k_d on the NO_2 concentration, and the invariance of k_d with respect to variations in the initial Cl concentration and excimer laser fluence indicate that reaction with NO_2 was the only important removal process for the adduct under the conditions of the experiments. The slope of the k_d versus [NO_2] plot (see Figure 7) defines the second-order rate coefficient $k_{15} = (2.70 \pm 0.17) \times 10^{-11}$ cm^3 molec^{-1} s^{-1} at 297 K and 155 Torr, where the uncertainty is 2σ and represents precision only. As was the case for the Cl−S(CH$_3$)$_2$ + NO rate coefficient measurement, we estimate that the absolute accuracy of this rate coefficient is ±15% at the 95% confidence level. The small positive intercept (4210 ± 2530 s^{-1}; uncertainty 2σ, precision only) may indicate a minor contribution of secondary chemistry to adduct removal at the lowest NO_2 concentrations. We estimate that the possible impact of secondary chemistry on the adduct decays observed at the lowest NO_2 concentrations would increase the reported rate coefficient by no more than a few percent.

Atmospheric Fate of Cl−S(CH$_3$)$_2$

The three processes most likely to be important destruction mechanisms for atmospheric Cl−S(CH$_3$)$_2$ are photodecomposition, reaction with O_2, and thermal decomposition:

$$\text{Cl}-\text{S(CH}_3\text{)}_2 + h\nu \rightarrow \text{products} \qquad (17)$$

$$\text{Cl}-\text{S(CH}_3\text{)}_2 + \text{O}_2 \rightarrow \text{products} \qquad (13)$$

$$\text{Cl}-\text{S(CH}_3\text{)}_2 \rightarrow \text{products} \qquad (-1)$$

Using the adduct UV−vis absorption spectrum measured in this

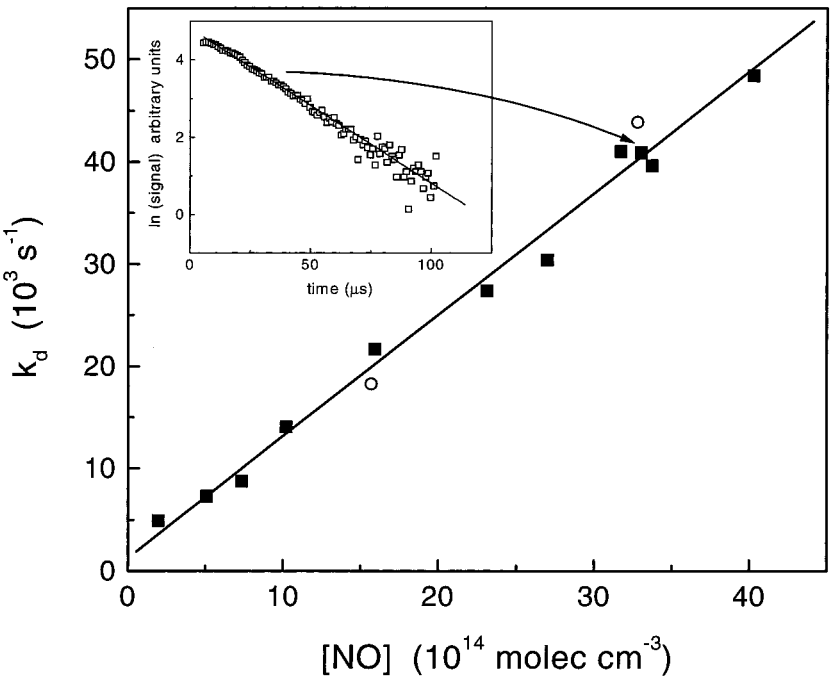

Figure 6. Plot of pseudo-first-order adduct decay rate (k_d) versus [NO] for data obtained at $T = 297$ K. Data acquired at (■) 155 Torr of N_2 and (○) 50 Torr of N_2. The solid line is a linear least-squares fit to the data. Best-fit slope is $(1.19 \pm 0.09) \times 10^{-11}$ cm^3 molec^{-1} s^{-1} (uncertainty is 2σ, precision only). Inset: a typical Cl−S(CH$_3$)$_2$ temporal profile. Line is a linear least-squares fit to the data. Total pressure = 155 Torr and $T = 297$ K. Reagent concentrations are (in units of 10^{13} molec cm^{-3}) [DMS] = 116, [NO] = 330, [Cl$_2$CO] = 193, and [Cl]$_0$ = 1.0. Best-fit slope (k_d) is 41 300 s^{-1}.

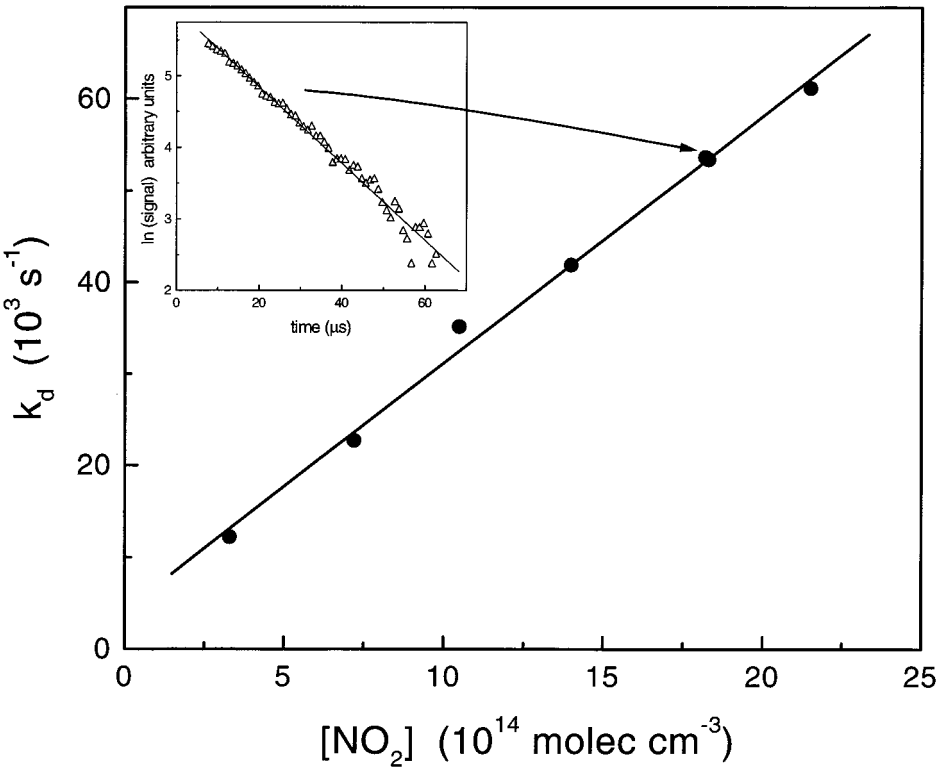

Figure 7. Plot of pseudo-first-order adduct decay rate (k_d) versus [NO$_2$] for data obtained at $T = 297$ K and $P = 155$ Torr in O$_2$ buffer gas. The solid line is a linear least-squares fit to the data. Best-fit slope is $(2.70 \pm 0.17) \times 10^{-11}$ cm^3 molec^{-1} s^{-1} (uncertainty is 2σ, precision only). Inset: a typical Cl−S(CH$_3$)$_2$ temporal profile. Line is a linear least-squares fit to the data. Reagent concentrations are (in units of 10^{13} molec cm^{-3}) [DMS] = 143, [NO$_2$] = 130, [Cl$_2$CO] = 593, and [Cl]$_0$ = 3.0. Best-fit slope (k_d) is 53 400 s^{-1}.

study, atmospheric photolysis rates, i.e., J values, have been calculated for the adduct using a global radiative transfer model.[31] Daily mean adduct J values corresponding to midwinter and midsummer, at latitudes of 0, 45 N, and 50 N, indicate that the adduct lifetime with respect to photodecomposition ranges from 3 to 18 s in the marine boundary layer (0−1 km), assuming a photodecomposition quantum yield of unity.

No evidence of reaction between the adduct and O$_2$ was observed in this study. Adduct temporal profiles observed in varied concentrations of O$_2$, suggest $k_{13} < 4 \times 10^{-18}$ cm^3

TABLE 3: Potential $Cl-S(CH_3)_2$ Photodecomposition Channels and Photolysis Wavelength Thresholds

photodecomposition channel	threshold wavelength (nm)
$Cl-S(CH_3)_2 + h\nu \rightarrow CH_3Cl + CH_3S$	3012
$\rightarrow HCl + CH_3SCH_2$	2891
$\rightarrow Cl + CH_3SCH_2$	1483
$\rightarrow CH_3 + CH_3SCl$	1048
$\rightarrow Cl + CH_3 + CH_3S$	307

molec^{-1} s^{-1}. Thus, the lower limit atmospheric lifetime of the adduct with respect to reaction with O_2 is ca. 0.05 s. However, it is likely that the true value for k_{13} is significantly lower than the upper limit obtained from our data.

If adduct reaction with O_2 is unimportant in the atmosphere, then thermal decomposition of the adduct may be the process that competes with or even dominates adduct photodecomposition. Theoretical calculations of the adduct energetics suggest adduct thermal decomposition rates of $k_{-1}(288\ K) \approx 2.5\ s^{-1}$ and $k_{-1}(298.15\ K) \approx 5\ s^{-1}$.[22] Another recent ab initio study of the Cl + DMS reaction[23] suggests that under atmospheric conditions thermal decomposition to reform Cl and DMS will be the only important atmospheric loss process for $Cl-S(CH_3)_2$. However, this conclusion is based on a calculated Cl−S bond dissociation energy of 51.5 kJ mol^{-1},[23] a value in agreement with an earlier calculation by McKee,[20] but significantly lower than that reported more recently by Wilson and Hirst[22] and McKee.[21] The $Br-S(CH_3)_2$ adduct bond energy has been measured experimentally and was found to be 59 ± 8 kJ mol^{-1}.[24] The $Br-S(CH_3)_2$ adduct is loosely bound at room temperature, possessing a lifetime on the order of 200 μs with respect to thermal dissociation to reform reactants.[24] The fact that at room temperature the $Cl-S(CH_3)_2$ adduct is stable on the millisecond time scale with respect to decomposition to reform Cl and DMS strongly suggests that the Cl−S bond strength of $Cl-S(CH_3)_2$ is significantly larger than the value calculated by Resende and De Almeida[23] and by McKee.[20]

The experiments of Stickel et al.[14] demonstrated that on the microsecond to millisecond time scale $Cl-S(CH_3)_2$ is stable with respect to thermal decomposition to produce either Cl or HCl. However, a thermal decomposition rate of only ca. 2 s^{-1} would dominate photodecomposition in the marine boundary layer, and neither the investigation of Stickel et al.[14] nor the current study, would have been sensitive to adduct decomposition on this time scale. Interestingly, the relative rate studies of Nielsen et al.[16] and Kinnison et al.[15] involved time scales of tens of minutes and may have been sensitive to adduct thermal decomposition. The fact that the relative rate studies of Nielsen et al.[16] and Kinnison et al.[15] both reported rate coefficients similar to that reported by Stickel et al.[14] indicates one of the following regarding the relative rate studies: (1) adduct decomposition did not occur on the time scale of the of these experiments, i.e., minutes; (2) the adduct thermal decomposition does not produce Cl + DMS; (3) under the conditions of the relative rate experiments, adduct self-reaction and adduct reaction with other radicals in the system were rapid enough to dominate adduct thermal decomposition and the major products of these reactions did not include DMS; or (4) adduct photodecomposition to products other than Cl + DMS dominated thermal decomposition under the conditions of the experiments.

Reaction with NO_x radicals could be an important loss process for $Cl-S(CH_3)_2$ in polluted regions of the marine boundary layer. At NO_x concentrations of 2 ppbv the adduct lifetime with respect to reaction with NO and NO_2 is ca. 1 s. Photolysis of $ClNO_2$, produced by heterogeneous processes, is believed to be an important source of Cl atoms in polluted areas of the marine boundary layer.[11] Thus, when present in sufficient concentration, under the appropriate circumstances, NO_x may serve as an agent that both produces and destroys $Cl-S(CH_3)_2$ in the marine environment.

In summary, atmospheric lifetimes of the $Cl-S(CH_3)_2$ adduct with respect to various processes are

photodecomposition: 3−20 s

thermal decomposition: highly uncertain

reaction with O_2: >0.05 s (highly uncertain)

reaction with NO and NO_2: 1 s

(for an NO_x mixing ratio of 2 ppbv)

The adduct was not observed to be reactive toward O_2; however, the results of the current study cannot rule out the possibility that the atmospheric fate of the adduct will be dominated by reaction with O_2. Kinnison et al.[16] observed a slightly larger rate coefficient for the Cl + DMS reaction in the presence of air than in the absence of O_2, i.e., $(3.61 \pm 0.21) \times 10^{-10}$ cm^3 molec^{-1} s^{-1} in 1 atm N_2 versus $(4.03 \pm 0.17) \times 10^{-10}$ cm^3 molec^{-1} s^{-1} in 1 atm of air, and attributed this to competition between adduct decomposition to reform reactants and adduct reaction with O_2.

If $Cl-S(CH_3)_2$ is sufficiently unreactive toward O_2 (i.e., if $k_{13} < 5 \times 10^{-20}$ cm^3 molec^{-1} s^{-1}), then adduct photodecomposition could be an important atmospheric removal process. Table 3 lists possible adduct photodecomposition pathways and associated photolysis wavelength thresholds. Photolysis to reform reactants would appear to be the most likely photodecomposition channel based on chemical considerations. However, production of the reactive sulfur species CH_3S and CH_3SCH_2 are more thermodynamically favorable pathways. While the reaction of Cl with DMS does not produce CH_3Cl directly,[18,19] it may generate this important compound in the atmosphere indirectly via $Cl-S(CH_3)_2$ formation and its subsequent photolysis.

Acknowledgment. This research was supported by the National Science Foundation through Grant ATM-94-12237. S. P. Urbanski received support from a NASA Earth System Science Fellowship. We thank H. Yu and S. Liu for calculating $Cl-S(CH_3)_2$ atmospheric photodissociation rates and J. M. Nicovich for helpful discussions and technical assistance.

References and Notes

(1) Berresheim, H.; Wine, P. H.; Davis, D. D. In *Composition, Chemistry and Climate of the Atmosphere*; Singh, H. B., Ed.; Van Nostrand Reinhold: New York, 1995; p 251.

(2) Bates, T. S.; Lamb, B. K.; Guenther, A.; Dignon, J.; Stoiber, R. E. *J. Atmos. Chem.* **1992**, *14*, 315.

(3) (a) Charlson, R. J.; Lovelock, J. E.; Andreae, M. O.; Warren, S. G. *Nature* **1987**, *326*, 655. (b) Shaw, G. E. *Climate Change* **1983**, *5*, 297.

(4) DeMore, W. B.; Sander, S. P.; Howard, C. J.; Ravishankara, A. R.; Golden, D. M.; Kolb, C. E.; Hampson, R. F.; Kurylo, M. J.; Molina, M. J. *Chemical Kinetics and Photochemical Data for Use in Stratospheric Modeling*; JPL Publication 97-4, No. 12; Pasadena, CA, 1997.

(5) Jobson, B. T.; Niki, H.; Yokouchi, Y.; Bottenheim, J.; Hopper, F.; Leaitch, R. *J. Geophys. Res.* **1994**, *99*, 25355.

(6) Singh, H. B.; Gregory, G. L.; Anderson, B.; Browell, E.; Sachse, G. W.; Davis, D. D.; Crawford, J.; Bradshaw, J. D.; Talbot, R.; Blake, D. R.; Thornton, D.; Newell, R.; Merrill, J. *J. Geophys. Res.* **1996**, *101*, 1907.

(7) Wingenter, O. W.; Kubo, M. K.; Blake, N. J.; Smith, T. W.; Blake, D. R.; Rowland, F. S. *J. Geophys. Res.* **1996**, *101*, 4331.

(8) Pszenny, A. A. P.; Keene, W. C.; Jacob, D. J.; Fan, S.; Maben, J. R.; Zetwo, M. P.; Springer-Young, M.; Galloway, J. N. *Geophys. Res. Lett.* **1993**, *20*, 699.

(9) Impey, G. A.; Shepson, P. B.; Hastie, D. R.; Barrie, L. A.; Anlauf, K. G. *J. Geophys. Res.* **1997**, *102*, 16005.

(10) Spicer, C. W.; Chapman, E. G.; Finlayson-Pitts, B. J.; Platridge, R. A.; Hubbe, J. M.; Fast, J. D.; Berkowitz, C. M. *Nature* **1998**, *394*, 353.

(11) Erickson, D. J.; Seuzaret, C.; Keene, W. C.; Gong, S. L. *J. Geophys. Res.* **1999**, *104*, 8347.

(12) Davis, D.; Chen, G.; Bandy, D.; Thornton, D.; Eisele, F.; Mauldin, L.; Tanner, D.; Lenschow, D.; Fuelberg, H.; Huebert, B.; Heath, J.; Clarke, A.; Blake, D. *J. Geophys. Res.* **1999**, *104*, 5765.

(13) Singh, H. B.; Thakur, A. N.; Chen, Y. E.; Kanakidou, M. *Geophys. Res. Lett.* **1996**, *23*, 1529.

(14) Stickel, R. E.; Nicovich, J. M.; Wang, S.; Zhao, Z.; Wine, P. H. *J. Phys. Chem.* **1992**, *26*, 9875.

(15) Kinnison, D. J.; Mengon, W.; Kerr, J. A. *J. Chem. Soc., Faraday Trans.* **1996**, *92*, 369.

(16) Nielsen, O. J.; Sidebottom, H. W.; Nelson, L.; Rattigan, O.; Treacy, J. J.; O'Farrell, D. J. *Int. J. Chem. Kinet.* **1990**, *22*, 603.

(17) Butkovskaya, N. I.; Le Bras, G. *J. Phys. Chem.* **1995**, *99*, 4536.

(18) Zhao, Z.; Stickel, R. E.; Wine, P. H. *Chem. Phys. Lett.* **1996**, *251*, 59.

(19) Langer, S.; McGoveny, B. T.; Finlayson-Pitts, B. J.; Moore, R. M. *Geophys. Res. Lett.* **1996**, *23*, 1661.

(20) McKee, M. L. *J. Phys. Chem.* **1993**, *97*, 10971.

(21) McKee, M. L. Personal communication, 1997.

(22) Wilson, C.; Hirst, D. M. *J. Chem. Soc., Faraday Trans.* **1997**, *93*, 2831.

(23) Resende, S. M.; De Almeida, W. B. *J. Phys. Chem. A* **1997**, *101*, 9738.

(24) Wine, P. H.; Nicovich, J. M.; Stickel, R. E.; Zhao, Z.; Shackelford, C. J.; Kreutter, K. D.; Daykin, E. P.; Wang, S. In *The Tropospheric Chemistry of Ozone in the Polar Regions;* Niki, H., Becker, K. H., Eds.; NATO ASI Series, Series I: Global Environmental Change, Vol. 7; 1993; pp 385−395.

(25) Ingham, T.; Bauer, D.; Sander, R.; Crutzen, P. J.; Crowley, J. N. *J. Phys. Chem. A* **1999**, *103*, 7199.

(26) Tyndall, G. S.; Cox, R. A.; Granier, C.; Lesclaux, R.; Moortgat, G. K.; Pilling, M. J.; Ravishankara, A. R.; Wallington, T. J. Review of the atmospheric chemistry of small organic peroxy radicals. To be published.

(27) Hearn, C. H.; Turco, E.; Joens, J. A. *Atmos. Environ.* **1990**, *24A*, 1939.

(28) Wallington, T. J.; Ellermann, T.; Nielsen, O. J. *J. Phys. Chem.* **1993**, *97*, 8442.

(29) Butkovskaya, N. I.; Le Bras, G. *J. Phys. Chem.* **1994**, *98*, 2582.

(30) Malleson, A. M.; Kellett, H. M.; Myhill, R. G.; Sweetenham, W. P. *A. E. R. E. Harwell Publication R 13729*; AERE Harwell Publications Office: Oxfordshire, UK, 1990.

(31) Yu, H.; Liu, S. Personal communication, 1999.

(32) Urbanski, S. P.; Stickel, R. E.; Zhao, Z.; Wine, P. H. *J. Chem. Soc., Faraday Trans.* **1997**, *93*, 2813.